

Charged black holes in quadratic gravity

Vojtěch Pravda^{*1}, Alena Pravdová^{†1}, and George Turner^{‡1,2}

¹Institute of Mathematics of the Czech Academy of Sciences,
Žitná 25, 115 67 Prague 1, Czech Republic

² Charles University, V Holešovičkách 2, 180 00 Prague 8, Czech Republic

June 11, 2024

Abstract

We study electrically charged, static, spherically symmetric black holes in quadratic gravity using the conformal-to-Kundt technique, which leads to a considerable simplification of the field equations. We study the solutions using a Frobenius-like approach of power-series expansions. The indicial equations restrict the set of possible leading powers to a few cases, describing, e.g., black holes, wormholes, or naked singularities.

We focus on the black hole case and derive recurrent formulas for all series coefficients of the infinite power-series expansion around the horizon. The solution is characterized by electric charge q , the black-hole radius a_0 , and the Bach parameter b related to the strength of the Bach tensor at the horizon. However, the Bach parameter has to be fine-tuned to ensure asymptotic flatness. The fine-tuning of b for a given q and a_0 returns up to two values, describing two branches of asymptotically flat, static, spherically symmetric, charged black holes in quadratic gravity. This is in agreement with previous numerical works.

We discuss various physical properties of these black holes, such as their asymptotic mass, temperature, photon spheres, and black-hole shadows. A straightforward generalization to dyonic black holes in quadratic gravity is also briefly mentioned.

1 Introduction

General relativity is currently our best theory of gravity, predicting and describing such fundamental physical phenomena as gravitational waves, cosmic expansion, and black holes. This classical theory of gravity, however, does not address quantum effects. From the effective field-theory view, higher-order correction terms should be added to the Einstein-Hilbert action. In this paper, we focus on quadratic gravity, where correction terms quadratic in the curvature are present.

Recently there has been considerable interest in spherically symmetric black holes in quadratic gravity, following early results of [1, 2]. It is well known that in four dimensions, Einstein spaces obey the vacuum field equations of quadratic gravity identically [3, 4]. The Schwarzschild black hole is, therefore, clearly a vacuum solution to quadratic gravity. Recently, however, it has been shown that

*pravda.math.cas.cz

†pravdova.math.cas.cz

‡turner.math.cas.cz

quadratic gravity also admits another static, spherically symmetric black hole solution over and above Schwarzschild [5, 6], violating the Birkhoff theorem of standard general relativity.

These non-Schwarzschild (or Schwarzschild-Bach) black holes admit one additional parameter - the Bach parameter b . However, the Bach parameter b has to be fine-tuned to ensure asymptotic flatness [5–8], leading effectively to a one-parameter family of asymptotically flat Schwarzschild-Bach black holes. In contrast, in the case of static, spherically symmetric black holes with non-vanishing cosmological constant Λ [9, 10], fine-tuning of the Bach parameter is not necessary since the Schwarzschild-Bach-(A)dS black holes are asymptotically (A)dS within certain continuous ranges of parameters, cf. [11, 12].

Recent works also studied the stability of static, spherically symmetric black holes in quadratic gravity. Long-wavelength instability of Schwarzschild-Bach black holes has been found [13] for horizon radii smaller than a critical value. Thus there seems to be a lower bound for the horizon radius of stable Schwarzschild-Bach black holes in quadratic gravity [13].

Charged, static, spherically symmetric black holes in quadratic gravity have been studied in [14, 15] using numerical methods. In this paper, we will study these black holes using the conformal-to-Kundt technique recently employed in [8–10, 12, 16]. This approach leads to a significant simplification of the field equations. This will enable us to find recurrent formulas for coefficients of power-series expansions of the metric functions and apply analytical techniques to the study of these black holes.

In Section 2, we revisit the electro-vacuum field equations of quadratic gravity and the conformal-to-Kundt approach.

In section 3, we derive the field equations in the Kundt coordinates. In passing, we also mention a straightforward generalization of the electrically charged black hole studied in this paper to the case of a dyonic black hole in quadratic gravity.

In section 4, we employ a Frobenius-like approach to solve the field equations in the Kundt coordinates in the vicinity of a generic hypersurface of constant radius. The field equations impose constraints on the dominant powers in the expansions, leading to a few allowed classes of static, spherically symmetric power-series solutions of quadratic gravity with electromagnetism. Besides black holes, these solutions may also represent wormholes and naked singularities. However, in this paper, we focus on the black-hole solutions.

In section 5, we concentrate on solutions admitting nonextremal horizons. We derive recurrent formulas for coefficients of power-series expansions of the metric. We observe that (at least for a certain range of parameters), the coefficients asymptotically approach a geometric series, which allows us to straightforwardly estimate the radii of convergence of the solutions.

Let us stress that in contrast with the vacuum case, where the Schwarzschild black hole solves the vacuum field equations of quadratic gravity, in the electrovacuum case, the Reissner-Nordström black hole does *not* obey the electrovacuum field equations. Instead, in agreement with the numerical results of [14, 15], we identify and study two branches of spherically symmetric, charged black holes. One represents charged Schwarzschild black holes in quadratic gravity (distinct from Reissner-Nordström), and the other one represents charged Schwarzschild-Bach black holes. In vacuum, the Schwarzschild and Schwarzschild-Bach black hole families intersect for a critical radius (e.g. $\bar{r}_0 \sim 0.876$, for parameters chosen in [6]). In the charged case, this is not always true, at least for a sufficiently large charge.

In section 5, we also study photon spheres and black-hole shadows of these charged black holes, benefiting from the simplification of photon-sphere and black-hole shadow description in the Kundt coordinates (as recently pointed out in [17]).

In section 6, we briefly discuss a case admitting an extremal horizon. Again, we provide recurrent

formulas for coefficients of power-series expansions of the corresponding metric. However, it seems much more difficult to fine-tune this case for asymptotic flatness. Therefore from our work, the existence of a charged, extremal, asymptotically flat black hole is inconclusive and will require further study.¹

Finally, for completeness, in the Appendix, we list the fine-tuned values of the Bach parameter for various values of charge and radius of the black hole.

2 Background

2.1 The quadratic gravity field equations

The action of quadratic gravity coupled with electromagnetism reads

$$S = \int d^4x \sqrt{-g} \mathcal{L} = \int d^4x \sqrt{-g} \left(\gamma R + \beta R^2 - \alpha C_{abcd} C^{abcd} - \frac{\kappa}{2} F_{ab} F^{ab} \right), \quad (1)$$

where $\gamma = 1/(16\pi G)$, G is the Newtonian constant (we will set $G = 1 = c$), and α, β are coupling constants of quadratic gravity.

The above action (1) leads to the following gravitational field equations

$$\gamma \left(R_{ab} - \frac{1}{2} R g_{ab} \right) - 4\alpha B_{ab} + 2\beta \left(R_{ab} - \frac{1}{4} R g_{ab} + g_{ab} \square - \nabla_b \nabla_a \right) R = \kappa T_{ab}, \quad (2)$$

where the energy-momentum tensor T_{ab} reads

$$T_{ab} = F_{ac} F_b{}^c - \frac{1}{4} g_{ab} F_{cd} F^{cd} \quad (3)$$

and B_{ab} is the Bach tensor

$$B_{ab} \equiv \left(\nabla^c \nabla^d + \frac{1}{2} R^{cd} \right) C_{acbd}. \quad (4)$$

The Bach tensor is traceless, symmetric, conserved, and well-behaved under conformal transformations of the metric tensor $g_{ab} = \Omega^2 \tilde{g}_{ab}$:

$$g^{ab} B_{ab} = 0, \quad B_{ab} = B_{ba}, \quad \nabla^b B_{ab} = 0, \quad B_{ab} = \Omega^{-2} \tilde{B}_{ab}. \quad (5)$$

Note that for Einstein spacetimes, the Bach tensor vanishes [18] and thus for these spacetimes, the vacuum field equations (eq. (2) with $T_{ab} = 0$) hold identically, making Einstein spacetimes, such as the Schwarzschild metric, trivial solutions of quadratic gravity as noted in Introduction. This ‘‘immunity’’ of Einstein spaces to the addition of quadratic gravity terms to the vacuum Einstein field equations, however, does not generalize to electrovacuum solutions of Einstein gravity. In particular, Reissner-Nordström black holes do not obey the quadratic gravity field equations with electromagnetism (2).

In the vacuum case, the trace no-hair theorem of [19], [6] states that for asymptotically flat, static, spherically symmetric black holes in quadratic gravity, the Ricci scalar R vanishes throughout the spacetime. Noting that the energy-momentum T_{ab} of an electromagnetic field is also traceless, it has been argued in [14] that the vanishing of R applies also to the electrovacuum case. This will be thus assumed in the rest of this paper.

¹In the numerical work of [14], it is stated that extremal black holes in this theory could exist in the Schwarzschild branch while not in the Schwarzschild-Bach branch.

The field equations (2) then reduce significantly to

$$R_{ab} - 4k B_{ab} = \kappa' T_{ab}, \quad (6)$$

where

$$k \equiv \frac{\alpha}{\gamma}, \quad \kappa' \equiv \frac{\kappa}{\gamma}, \quad (7)$$

assuming $\gamma \neq 0$.

2.2 Conformal-to-Kundt ansatz

Instead of using the standard spherically symmetric metric

$$ds^2 = -h(\bar{r}) dt^2 + \frac{d\bar{r}^2}{f(\bar{r})} + \bar{r}^2 d\omega^2, \quad d\omega^2 = d\theta^2 + \sin^2 \theta d\phi^2, \quad (8)$$

we will employ its conformal-to-Kundt form [8, 16, 20]

$$ds^2 \equiv \Omega^2(r) ds_K^2 = \Omega^2(r) \left[d\omega^2 - 2 du dr + \mathcal{H}(r) du^2 \right], \quad (9)$$

which leads to a considerable simplification of the field equations.

This metric admits a gauge freedom

$$r \rightarrow \lambda r + v, \quad u \rightarrow \lambda^{-1} u, \quad (10)$$

where λ, v are constants. In addition, the metric (8) admits also a time-scaling freedom

$$t \rightarrow t/\sigma \Rightarrow h \rightarrow h\sigma^2, \quad (11)$$

where the constant $\sigma \neq 0$ can be used to adjust value of h at a chosen radius \bar{r} .

The standard metric form (8) can be obtained (assuming $\Omega' \neq 0 \neq \mathcal{H}$) by [20]

$$\bar{r} = \Omega(r), \quad t = u - \int \frac{dr}{\mathcal{H}(r)}, \quad (12)$$

leading to

$$h = -\Omega^2 \mathcal{H}, \quad f = -\left(\frac{\Omega'}{\Omega}\right)^2 \mathcal{H}, \quad (13)$$

where a prime denotes differentiation with respect to r .

The Killing horizon, where the Killing vector field $\partial_u = \partial_t$ becomes null, is located at the zeros $r = r_h$ of the metric function \mathcal{H} ,

$$\mathcal{H}|_{r=r_h} = 0. \quad (14)$$

Then using (13), also $h(\bar{r}_h) = 0 = f(\bar{r}_h)$, where $\bar{r}_h = \Omega(r_h)$.

Curvature invariants constructed from the Bach and Weyl tensors have the same form for vacuum [8] and charged case

$$B_{ab} B^{ab} = \frac{1}{72} \Omega^{-8} [(\mathcal{B}_1)^2 + 2(\mathcal{B}_1 + \mathcal{B}_2)^2], \quad (15)$$

$$C_{abcd} C^{abcd} = \frac{1}{3} \Omega^{-4} (\mathcal{H}'' + 2)^2, \quad (16)$$

where

$$\mathcal{B}_1 \equiv \mathcal{H}\mathcal{H}'''' , \quad (17)$$

$$\mathcal{B}_2 \equiv \mathcal{H}'\mathcal{H}''' - \frac{1}{2}\mathcal{H}''^2 + 2 . \quad (18)$$

Note that the Kundt coordinates are also useful for the description of conformally invariant properties of spacetimes, such as photon spheres, see sec. 5.1.2.

2.2.1 The Reissner-Nordström black hole

Recall that the Schwarzschild metric is a vacuum solution of quadratic gravity. In contrast, the Reissner-Nordström metric is not a solution of electrovacuum quadratic gravity (6), (3). Nevertheless, it will be useful for comparison with actual solutions.

In the Kundt coordinates, the Reissner-Nordström metric functions read

$$\Omega(r) = -\frac{1}{r}, \quad \mathcal{H}(r) = -r^2 - 2Mr^3 - \frac{Q^2}{4\pi\epsilon_0}r^4 . \quad (19)$$

In the vicinity of a horizon, which is located at a non-zero root of $\mathcal{H}(r_h) = 0$, eq. (19) gives

$$\begin{aligned} \mathcal{H}(r) = & - \left(2 + 6Mr_h + \frac{Q^2}{\pi\epsilon_0}r_h^2 \right) r_h(r - r_h) - \frac{1}{2} \left(2 + 12Mr_h + 3\frac{Q^2}{\pi\epsilon_0}r_h^2 \right) (r - r_h)^2 \\ & - \left(2M + \frac{Q^2}{\pi\epsilon_0}r_h \right) (r - r_h)^3 - \frac{Q^2}{4\pi\epsilon_0}(r - r_h)^4 . \end{aligned} \quad (20)$$

3 The field equations in Kundt coordinates

3.1 Maxwell equations

In agreement with the previous works [14,15], we start with the following ansatz for the electromagnetic field

$$\mathbf{A} = \bar{A}(\bar{r})dt, \quad (21)$$

which in the Kundt coordinates reads

$$\mathbf{A} = A(r)du - \frac{A(r)}{\mathcal{H}(r)}dr. \quad (22)$$

The Maxwell equations then reduce to

$$A'' = 0 \quad (23)$$

and thus in the Kundt coordinates, they can be solved exactly as

$$A = qr \quad (24)$$

(the constant term can be removed by a gauge transformation). In contrast, the fundamental electromagnetic invariant $F_{ab}F^{ab}$ can be expressed exactly in the physical coordinates and turns out to be the same as in the Reissner-Nordström case

$$F_{ab}F^{ab} = -\frac{2q^2}{\Omega^4} = -\frac{2q^2}{\bar{r}^4}. \quad (25)$$

Note that the stress-energy tensor (3) and thus the full system of the field equations is invariant under the $SO(2)$ group of electric-magnetic duality. It is thus straightforward to construct a dyonic black hole in quadratic gravity by adding the term $\mathcal{B}(\theta)d\phi$ to the potential (21). Maxwell equations then imply $\mathcal{B}(\theta) = \beta \cos \theta$, where β is magnetic charge (the metric remains unchanged except for replacing q^2 by $q^2 + \beta^2$). This is analogous to the case of the Einstein-Maxwell system, where the dyonic generalization of Reissner-Nordström black hole admitting both electric and magnetic charges was constructed in [21] (cf also [22]).

3.2 Gravitational field equations

Following the same approach as in the previous works [8–10, 16] for quadratic gravity in vacuum, we find that the quadratic gravity field equations (6) in the Kundt coordinates (9) reduce to the following system of two autonomous ordinary differential equations

$$\Omega\Omega'' - 2\Omega'^2 = \frac{1}{3}k\mathcal{H}'''' , \quad (26)$$

$$\Omega\Omega'\mathcal{H}' + 3\Omega'^2\mathcal{H} + \Omega^2 = \frac{1}{3}k(\mathcal{H}'\mathcal{H}''' - \frac{1}{2}\mathcal{H}''^2 + 2) + \frac{\kappa'}{2}q^2 . \quad (27)$$

Occasionally, it is also useful to use the trace of the field equations which follows from the two above equations

$$\mathcal{H}\Omega'' + \mathcal{H}'\Omega' + \frac{1}{6}(\mathcal{H}'' + 2)\Omega = 0 . \quad (28)$$

Note that the only difference from the vacuum case is the term proportional to q^2 appearing in (27).

4 Expansion of the metric in powers of r around any fixed finite value r_0

In this section, we expand the metric functions $\Omega(r)$ and $\mathcal{H}(r)$ in powers of $\Delta \equiv r - r_0$ around some fixed, finite value r_0 . The field equations (26), (27) impose constraints on the dominant powers in the expansions, leading to a limited number of allowed classes of static, spherically symmetric power-series solutions of quadratic gravity with electromagnetism summarized in Table 1.

4.1 Expansion in powers of Δ

Now, let us solve (26), (27) using expansions in powers of Δ around an arbitrary, finite, fixed value r_0 ,

$$\Omega(r) = \Delta^n \sum_{i=0}^{\infty} a_i \Delta^i , \quad (29)$$

$$\mathcal{H}(r) = \Delta^p \sum_{i=0}^{\infty} c_i \Delta^i , \quad (30)$$

where r_0 , n , and p are real numbers. We also assume that the leading coefficients are non-vanishing, i.e., $a_0 \neq 0$, $c_0 \neq 0$. Note that while the steps in Δ are integer it might not be so in the physical coordinate \bar{r} , see e.g., [16].

Substituting the series (29), (30) into the field equations (26), (27), and the trace equation (28), yields

$$\begin{aligned} & \sum_{l=2n-2}^{\infty} \Delta^l \sum_{i=0}^{l-2n+2} a_i a_{l-i-2n+2} (l-i-n+2)(l-3i-3n+1) \\ &= \frac{1}{3}k \sum_{l=p-4}^{\infty} \Delta^l c_{l-p+4} (l+4)(l+3)(l+2)(l+1), \end{aligned} \quad (31)$$

$$\begin{aligned} & \sum_{l=2n+p-2}^{\infty} \Delta^l \sum_{j=0}^{l-2n-p+2} \sum_{i=0}^j a_i a_{j-i} c_{l-j-2n-p+2} (j-i+n)(l-j+3i+n+2) + \sum_{l=2n}^{\infty} \Delta^l \sum_{i=0}^{l-2n} a_i a_{l-i-2n} \\ &= \frac{1}{3}k \left[2 + \sum_{l=2p-4}^{\infty} \Delta^l \sum_{i=0}^{l-2p+4} c_i c_{l-i-2p+4} (i+p)(l-i-p+4)(l-i-p+3)(l-\frac{3}{2}i-\frac{3}{2}p+\frac{5}{2}) \right] + \frac{\kappa' q^2}{2}, \end{aligned} \quad (32)$$

and

$$\sum_{l=n+p-2}^{\infty} \Delta^l \sum_{i=0}^{l-n-p+2} c_i a_{l-i-n-p+2} \left[(l-i-p+2)(l+1) + \frac{1}{6}(i+p)(i+p-1) \right] + \frac{1}{3} \sum_{l=n}^{\infty} \Delta^l a_{l-n} = 0. \quad (33)$$

respectively.

By a careful study of leading orders of equations (31)-(33), it turns out that only certain combinations of exponents n, p appearing in the expansion of metric functions $\Omega(r)$ and $\mathcal{H}(r)$, (29), (30), are allowed. The resulting classes $[n, p]$ are summarized in Table 1.

$[n, p]$	constraints	free parameters	physical region
$[-1, 2]$	$c_0 = -1$	a_0, c_1, r_0, q	$\bar{r} \rightarrow \infty$
$[0, 1]$		$a_0, c_0, c_1, r_0 = r_h, q$	$\bar{r} \rightarrow \bar{r}_h = a_0$
$[0, 0]$		$a_0, a_1, c_0, c_1, c_2, r_0, q$	$\bar{r} \rightarrow \bar{r}_0 = a_0$
$[0, 2]$	$c_0 = -1, a_0^2 = \frac{\kappa'}{2}q^2$	$c_1, r_0 = r_h, q$	$\bar{r} \rightarrow \bar{r}_h = a_0$
$[1, 0]$		$a_0, c_0, c_1, c_2, r_0, q$	$\bar{r} \rightarrow 0$
$[n > 0, 2]$	$c_0^2 = 1 + \frac{3\kappa'}{4k}q^2, q^2 = -\frac{4kn(n+1)[3n(n+1)+2]}{\kappa'[3n(n+1)+1]^2},$ $(3n^2 + 3n + 1)c_0 = -1$ for $\frac{\kappa'}{k} > -\frac{4}{3q^2}$	a_0, c_1, r_0	$\bar{r} \rightarrow 0$

Table 1: All possible classes $[n, p]$ of static, spherically symmetric solutions to quadratic gravity coupled with electromagnetism that can be expressed as power series (29), (30). Note that these classes may admit special subclasses. For example, the case $[0, 2]$ has special subcases for $c_1 = 0$, such as c_2 arbitrary and $a_0^2 = \kappa' q^2 / 2 = 12k$, or $c_1 = c_2 = 0$, c_3 arbitrary and $a_0^2 = \kappa' q^2 / 2 = 24k$, or in general $c_1 = c_2 = \dots = c_{l-1} = 0$, c_l arbitrary and $a_0^2 = \kappa' q^2 / 2 = 2kl(l+1)$.

Distinct classes $[n,p]$ may or may not correspond to the same branch of solutions in different regions of a spacetime. For example, class $[0,1]$ describing near-horizon metric and class $[0,0]$ with appropriately chosen parameters describing the metric near a generic point outside the horizon may represent the same physical solution. At the same time, class $[0,0]$ with a different choice of parameters can correspond to a generic point outside of a wormhole or naked singularity, see [16].

In this paper, we are interested in cases describing black-hole solutions to quadratic gravity in the vicinity of a horizon. Thus in the rest of the paper, we will focus on the classes $[0,1]$ and $[0,2]$, for which $\mathcal{H} = 0$ at $r_0 = r_h$ (14), corresponding to non-extremal/extremal horizon, respectively. Moreover, it seems that the case $[0,2]$ is not asymptotically flat (see section 6). Thus, the most physically relevant case is $[0,1]$.

5 Charged black holes with non-extremal horizons (case $[0,1]$)

So far, in section 4, we employed the leading orders of equations (31)-(33). Now let us focus on the case corresponding to the solution in the vicinity of a non-extremal horizon, set $[n,p] = [0,1]$, and study conditions following from higher orders in eqs. (31)-(33) (or equivalently (26), (27), and (28)).

The lowest nontrivial order of the trace equation (28) gives

$$a_1 = -\frac{a_0}{3c_0}(c_1 + 1). \quad (34)$$

Then the lowest nontrivial order of (27) reduces to

$$c_2 = \frac{1}{6kc_0} [2k(c_1^2 - 1) + a_0^2(2 - c_1)] - \frac{q^2\kappa'}{4c_0k}. \quad (35)$$

All higher-order coefficients can be expressed via recurrent formulas

$$c_{l+2} = \frac{3}{k(l+3)(l+2)(l+1)l} \sum_{i=0}^l a_i a_{l+1-i} (l+1-i)(l-3i) \quad \forall l \geq 1, \quad (36)$$

$$a_l = \frac{1}{l^2 c_0} \left[-\frac{1}{3} a_{l-1} - \sum_{i=1}^l c_i a_{l-i} [l(l-i) + \frac{1}{6} i(i+1)] \right] \quad \forall l \geq 2, \quad (37)$$

where a_0 , c_0 , c_1 , and q are arbitrary constant parameters. Note that the form of the recurrent expressions (36), (37) is identical to the uncharged case [16] since charge enters only via c_2 in (35).

On the horizon, the Bach and Weyl invariants (15), and (16), read

$$B_{ab} B^{ab}(r_h) = \left(\frac{2a_0^2(c_1 - 2) + 3\kappa'q^2}{12a_0^4k} \right)^2 = \left(\frac{2a_0^2b + \kappa'q^2}{4a_0^4k} \right)^2, \quad (38)$$

$$C_{abcd} C^{abcd}(r_h) = \frac{[2(c_1 + 1)]^2}{3a_0^4} = 3 \left(\frac{2(b+1)}{a_0^2} \right)^2, \quad (39)$$

respectively, where, similarly as in the vacuum case, we introduce a dimensionless Bach parameter b measuring the strength of the Bach tensor at the horizon when $q = 0$ by

$$b \equiv \frac{1}{3} (c_1 - 2). \quad (40)$$

Note that the invariant (38) vanishes either for $b = 0 = q$, which corresponds to the Schwarzschild solution, or for $b = -\kappa'q^2/(2a_0^2)$.

Then a few terms in the expansions (29) and (30) read

$$\mathcal{H} = c_0(r - r_h) + (3b + 2)(r - r_h)^2 + \frac{12kb^2 + 2b(8k - a_0^2) + 4k - \kappa'q^2}{4kc_0}(r - r_h)^3 + \dots, \quad (41)$$

$$\Omega = a_0 - \frac{a_0(b + 1)}{c_0}(r - r_h) + \frac{a_0}{16kc_0^2} [16(b + 1)^2k + 2a_0^2b + \kappa'q^2] (r - r_h)^2 + \dots. \quad (42)$$

Therefore, using (12), in physical coordinates, the horizon is located at²

$$\bar{r}(r_h) = \Omega(r_h) = \bar{r}_h = a_0 > 0, \quad (43)$$

where both metric functions f and h vanish (c.f. (13)).

Using (10), one can also set $a_1 > 0$, to ensure monotonic increasing of \bar{r} as a function of r in the vicinity of the horizon. Finally, for studying solutions around the outer black hole horizon, we assume $c_0 < 0$ (see [12]). To summarize,

$$a_0, a_1 > 0, \quad c_0 < 0. \quad (44)$$

It turns out that similarly as in the vacuum case [5,6,8], for a generic value of the Bach parameter b , the metric (8) expressed using the expansions (29), (30) and the recurrent formulas (36) and (37) is not asymptotically flat. However, for given specific values of parameters, the parameter b can be fine-tuned to obtain asymptotically flat cases. Let us thus now present examples of [0,1] solutions for some specific values of parameters.

We will choose

$$r_0 = -1, \quad k = 1/2, \quad c_0 = -1, \quad a_0 = 1, \quad \kappa' = 1, \quad (45)$$

together with a selected value of charge q and corresponding fine-tuned values of b . For $q < \approx 0.91$ there will be two such values of b . The corresponding two branches of solutions represent charged Schwarzschild³ and charged Schwarzschild-Bach solutions in quadratic gravity.

First note that often, the series a_i and c_i asymptotically approach geometric series⁴ (see Figure 1). This will allow us to estimate the radius of convergence of the series.

The behavior of the metric functions $\Omega(r)$ and $\mathcal{H}(r)$ for parameters (45), $q = 0.5$, and $b = 0.6314924332806$ is shown in Figures 2 and 3, respectively. Using (13), one can also express the metric functions $f(\bar{r})$ and $h(\bar{r})$ in the physical coordinates, see Figures 4 and 5, respectively. Note that the function $h(\bar{r})$ is re-scaled to approach 1 at large \bar{r} .

The high precision needed for fine-tuning the Bach parameter b is illustrated by Figures 6 and 7. Both figures correspond to the same parameters (45) and $q = 0.5$, but are fine-tuned for distinct values of b . Figure 6 corresponds to the charged Schwarzschild-Bach black hole while Figure 7 corresponds to the charged Schwarzschild black hole.

These two branches of solutions, charged Schwarzschild and charged Schwarzschild-Bach, are shown in Figure 8.

²Note that without loss of generality, the sign of a_0 can be chosen thanks to the invariance of (9) under the sign change $\Omega \rightarrow -\Omega$.

³Recall that charged Schwarzschild in quadratic gravity is distinct from Reissner-Nordström metric which is not a solution of quadratic gravity with Maxwell field.

⁴If the series a_i and c_i do not asymptotically approach geometric series, more general criteria have to be used for determining convergence of the series. For example, in this context, the root test for convergence is employed in [17].

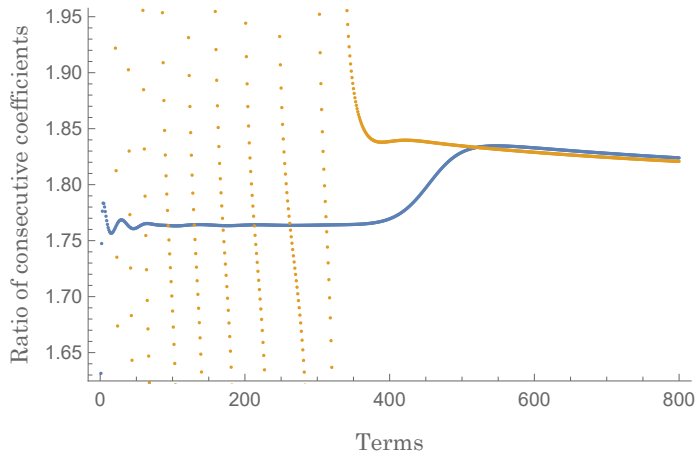


Figure 1: Ratios of consecutive coefficients, a_i/a_{i-1} (blue) and c_i/c_{i-1} (yellow), in the expansions of metric functions (29), (30), using the parameters (45) with $b = 0.6314924332806$ and $q = 0.5$.

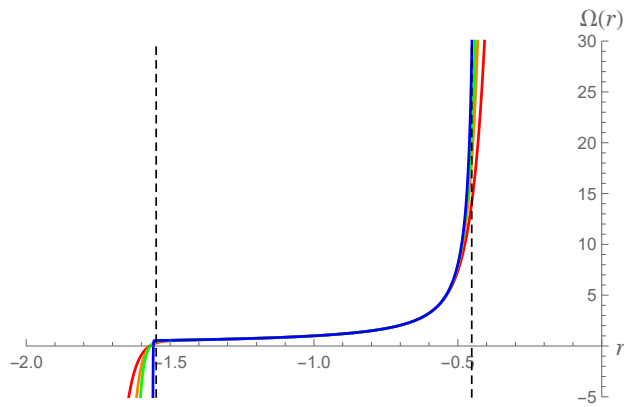


Figure 2: The metric function $\Omega(r)$, using the parameters (45) with $b = 0.6314924332806$ and $q = 0.5$, for the first 20 (red), 30 (orange), 40 (green), and 800 (blue) terms. The vertical dashed lines indicate the interval of convergence of the series ($r_0 \pm 1/p$ where p is the value converged upon in Figure 1).

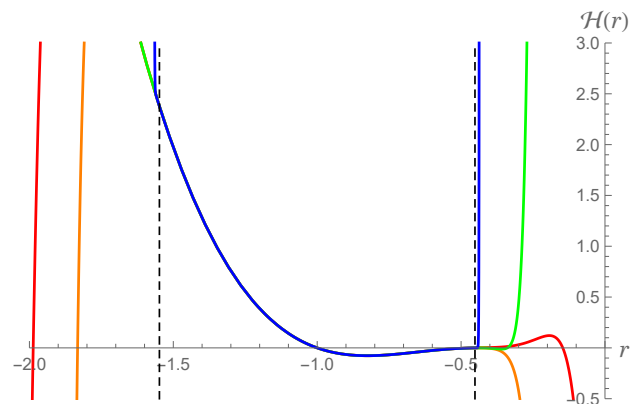


Figure 3: The metric function $\mathcal{H}(r)$, using the parameters (45) with $b = 0.6314924332806$ and $q = 0.5$, for the first 20 (red), 30 (orange), 40 (green), and 800 (blue) terms. The vertical dashed lines indicate the interval of convergence of the series as in Figure 2.

5.1 Some physical properties of charged [0,1] black holes

In this section, we study selected physical properties of charged [0,1] black holes. These include mass, temperature, the radius of the photon sphere, and the black-hole shadow.

Recall that the metric function h of the [0,1] black hole obtained from the recurrent formulas (36), (37) with the Bach parameter b fine-tuned for asymptotic flatness and transformed to physical coordinates is in general asymptotically approaching a constant distinct from 1. To set the asymptotic value of h to 1 we employ the scaling freedom (11). This will fix the value of σ for each specific asymptotically flat [0,1] black hole.

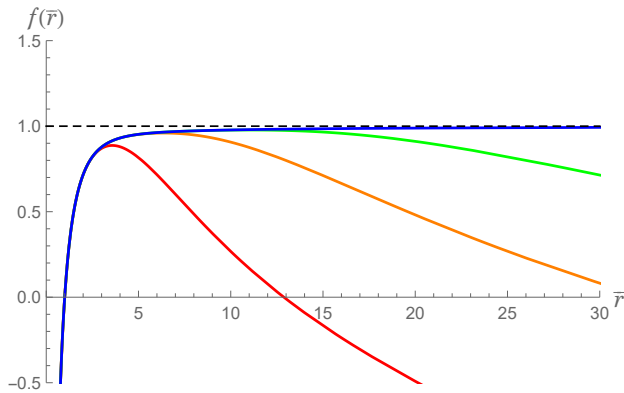


Figure 4: The metric function $f(\bar{r})$, using the parameters (45) with $b = 0.6314924332806$ and $q = 0.5$, for the first 20 (red), 50 (orange), 100 (green), and 800 (blue) terms.

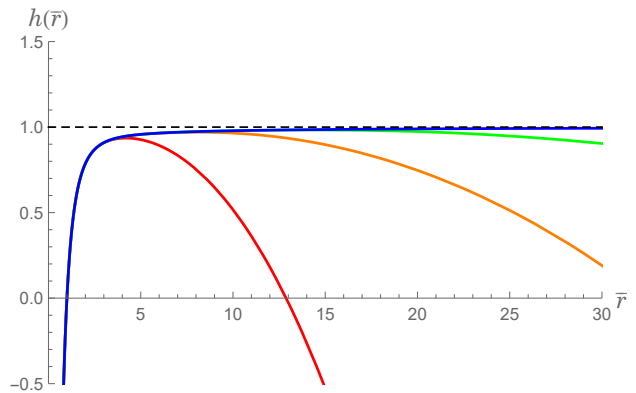


Figure 5: The metric function $h(\bar{r})$, using the parameters (45) with $b = 0.6314924332806$ and $q = 0.5$, re-scaled to approach 1 at large \bar{r} . The first 20 (red), 50 (orange), 100 (green), and 800 (blue) terms of the expansion are shown.

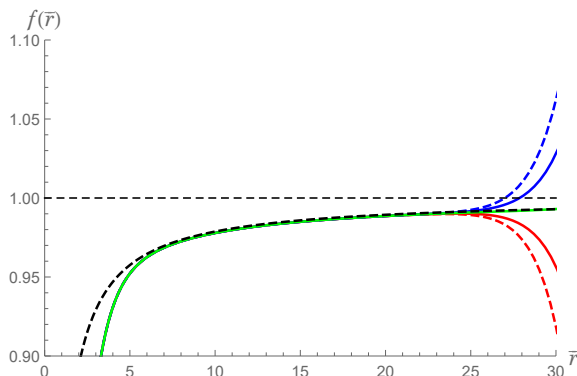


Figure 6: The metric function $f(\bar{r})$ of charged Schwarzschild-Bach solution for various values of b using the parameters (45) and $q = 0.5$: $b = 0.6314924332804$ (blue, dashed); $b = 0.6314924332805$ (blue, solid); $b = 0.6314924332807$ (red, solid); $b = 0.6314924332808$ (red, dashed); and the most finely-tuned $b = 0.6314924332806$ in green. The black, dashed line represents the function $1 - 2M/\bar{r}$ where $2M \approx 0.212$: the mass determined from the asymptotic behaviour of $h(\bar{r})$.

5.1.1 Asymptotic mass, horizon area, surface gravity and temperature

Asymptotic mass M can be determined by comparing the metric function $f(\bar{r})$ or the re-scaled metric function $h(\bar{r})$ with $1 - 2M/\bar{r}$. See Figure 9 for the dependence of asymptotic mass M on charge q for both branches of asymptotically flat $[0, 1]$ black holes. Note that while for the Schwarzschild branch, asymptotic mass increases with charge, for Schwarzschild-Bach it decreases and reaches negative values for sufficiently large charge.⁵ This can be also seen in Figure 10.

In most figures, we keep the horizon radius $\bar{r}_h = a_0$, cf. (43), fixed by (45). However, it is also of

⁵Note, however, that for sufficiently small a_0 , this behavior is interchanged, e.g., for the Schwarzschild branch, the asymptotic mass decreases with increasing charge, see [15].

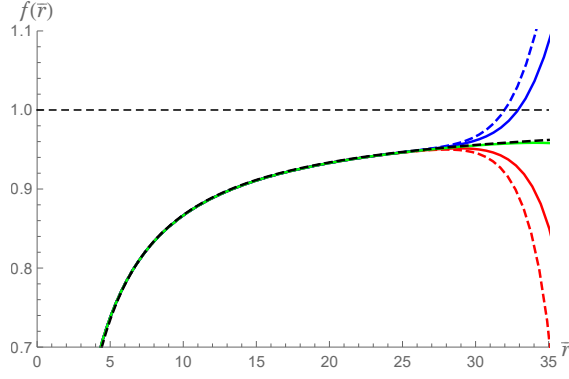


Figure 7: The metric function $f(\bar{r})$ of charged Schwarzschild solution for various values of b using the parameters (45) and $q = 0.5$: $b = -0.269102353931866$ (blue, dashed); $b = -0.269102353931867$ (blue, solid); $b = -0.269102353931869$ (red, solid); $b = -0.26910235393187$ (red, dashed); and the most finely-tuned $b = -0.269102353931868$ in green. The black, dashed line represents the function $1 - 2M/\bar{r}$ where $2M \approx 1.327$: the mass determined from the asymptotic behaviour of $h(\bar{r})$.

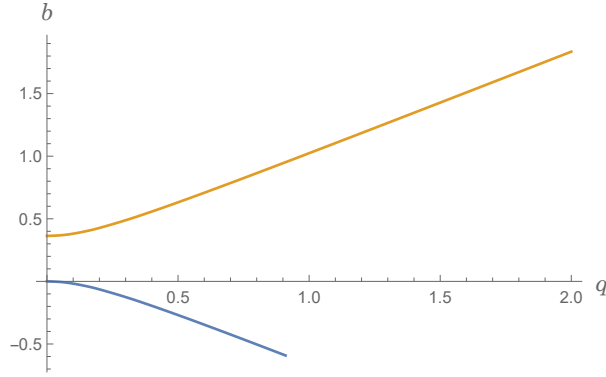


Figure 8: Finely-tuned Bach parameters b corresponding to asymptotically flat solutions (with parameters (45)) as functions of charge q . The charged Schwarzschild branch (blue) truncates around $q \approx 0.91$ while the charged Schwarzschild-Bach branch (yellow) permits asymptotically flat solutions with greater charge.

interest to study the dependence of the asymptotic mass M on the horizon radius $\bar{r}_h = a_0$, see Figures 11 and 12 for the uncharged and charged case, respectively.

The null Killing vector $\xi \equiv \sigma \partial_u = \sigma \partial_t$ generates the horizon. The location of which is given by vanishing of the norm of ξ , i.e., by $\mathcal{H}(r) = 0$ at $r = r_h$, using (41). The horizon area reads

$$\mathcal{A} = 4\pi \Omega^2(r_h) = 4\pi a_0^2 = 4\pi \bar{r}_h^2. \quad (46)$$

The surface gravity $\kappa^2 \equiv -\frac{1}{2} \xi_{\mu;\nu} \xi^{\mu;\nu}$ [23], where the only nonvanishing derivatives of ξ are $\xi_{u;r} = -\xi_{r;u} = \frac{1}{2} \sigma (\Omega^2 \mathcal{H})'$, $\xi^{r;u} = -\xi^{u;r} = \Omega^{-4} \xi_{u;r}$, using (41), reads

$$\kappa/\sigma = -\frac{1}{2} (\mathcal{H}' + 2\mathcal{H} \Omega'/\Omega)|_{r=r_h} = -\frac{1}{2} \mathcal{H}'(r_h) = -\frac{1}{2} c_0. \quad (47)$$

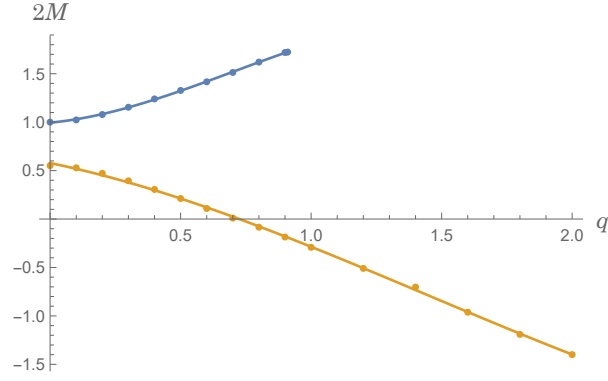


Figure 9: Asymptotic mass as a function of charge q , determined by fitting the model $1 - 2M/\bar{r}$ to the re-scaled metric function $h(\bar{r})$ (see Figure 5) over an appropriate range of \bar{r} . Charged Schwarzschild solutions are in blue while charged Schwarzschild-Bach solutions are in yellow. All solutions make use of the parameters (45).

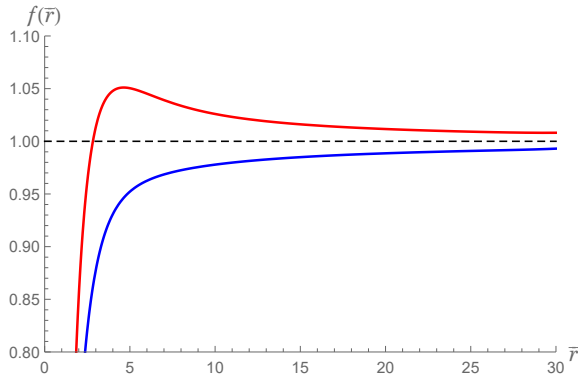


Figure 10: $f(\bar{r})$ for two charged Schwarzschild-Bach solutions using the parameters (45): one with positive mass, $q = 0.5$ and tuned to $b = 0.6314924332806$ (blue); the other with negative mass, $q = 1$ and tuned to $b = 1.02395913547716$ (red).

Then the temperature of the black hole horizon $T \equiv \kappa/(2\pi)$ [24] is given by

$$T/\sigma = -\frac{1}{4\pi}c_0. \quad (48)$$

Figure 13 shows the dependence of temperature on charge for both branches of black holes.

5.1.2 Photon sphere and black hole shadow

In this section, we study photon spheres and black-hole shadows for asymptotically flat, spherically symmetric, charged black holes in quadratic gravity.

In the physical coordinates (8), the photon sphere⁶ is located at $2h = \bar{r}h_{,\bar{r}}$, i.e.,

$$\left(\frac{h}{\bar{r}^2}\right)_{,\bar{r}} = 0. \quad (49)$$

⁶For the definition of photon spheres for static, spherically symmetric spacetimes in standard coordinates (8), see [25].

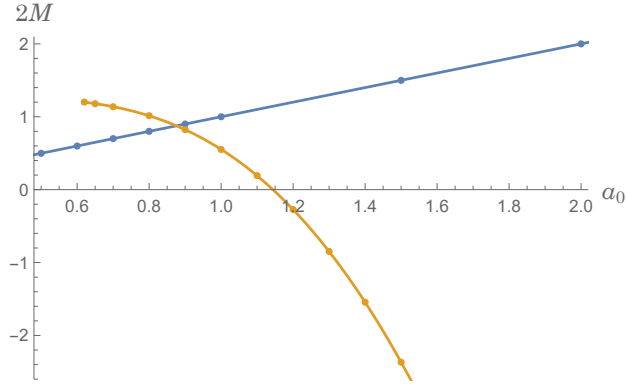


Figure 11: Asymptotic mass of Schwarzschild (blue) and uncharged Schwarzschild-Bach (yellow) black holes as functions of the horizon radius $\bar{r}_h = a_0$, cf. (43). This figure corresponds to previously published Figure 3 of [6].

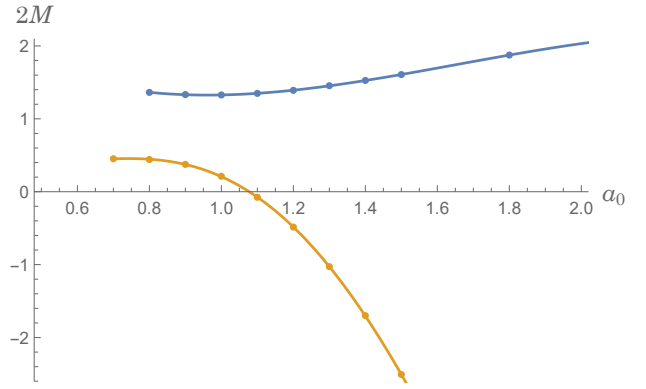


Figure 12: Asymptotic mass of charged Schwarzschild (blue) and Schwarzschild-Bach (yellow) black holes with charge $q = 0.5$ as functions of the horizon radius $\bar{r}_h = a_0$, cf. (43).

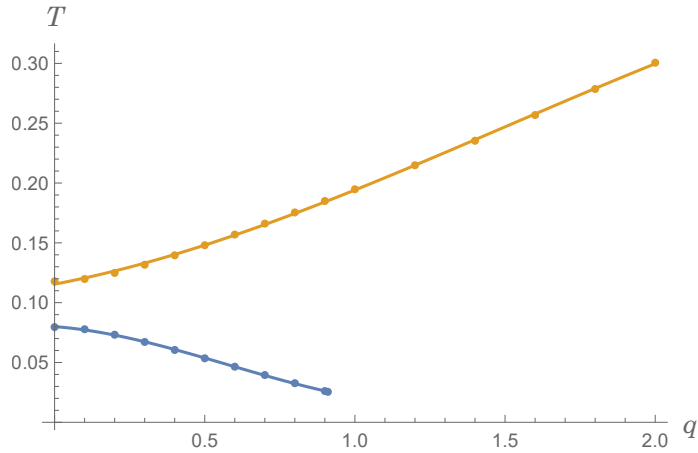


Figure 13: Temperature as a function of charge q for charged Schwarzschild solutions (blue) and charged Schwarzschild-Bach solutions (yellow). All solutions make use of the parameters (45).

As pointed out in [17], the Kundt coordinates (9) are more suitable for the study of photon spheres. In these coordinates, using (13), (49) reduces to [17]

$$\mathcal{H}_{,r}(r_{\text{ps}}) = 0, \quad (50)$$

provided $\mathcal{H}(r_{\text{ps}}) < 0$ and $\Omega_{,r}(r_{\text{ps}}) \neq 0$. Photon spheres in fact correspond to local maxima of the metric function $-\mathcal{H}$, see Figures 14 and 15 for charged Schwarzschild and charged Schwarzschild-Bach black holes with different charges, respectively.

The shadow of an asymptotically flat, spherically symmetric black hole is a disk of a radius $\bar{r}_{\text{sh}} = \frac{\bar{r}_{\text{ps}}}{\sqrt{h(\bar{r}_{\text{ps}})}}$ (see (2.14) of [26]). In the Kundt coordinates, this reads

$$\bar{r}_{\text{sh}} = \frac{1}{\sigma \sqrt{|\mathcal{H}(r_{\text{ps}})|}}. \quad (51)$$

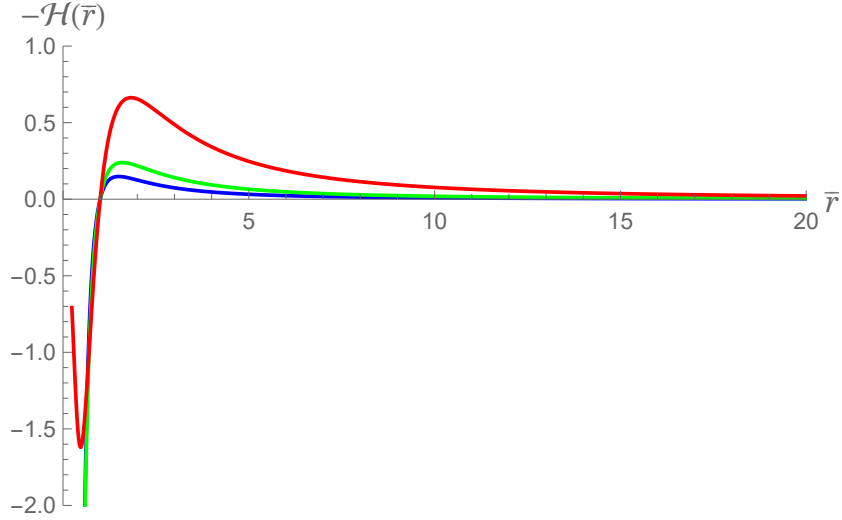


Figure 14: $-\mathcal{H}(\bar{r})$ for various charged Schwarzschild black holes using the parameters (45): blue ($q = 0$, $b = 0$), green ($q = 0.5$, $b = -0.269102353931868$), and red ($q = 0.9$, $b = -0.583718480513498$). This functions as an effective potential for null geodesics around the black hole.

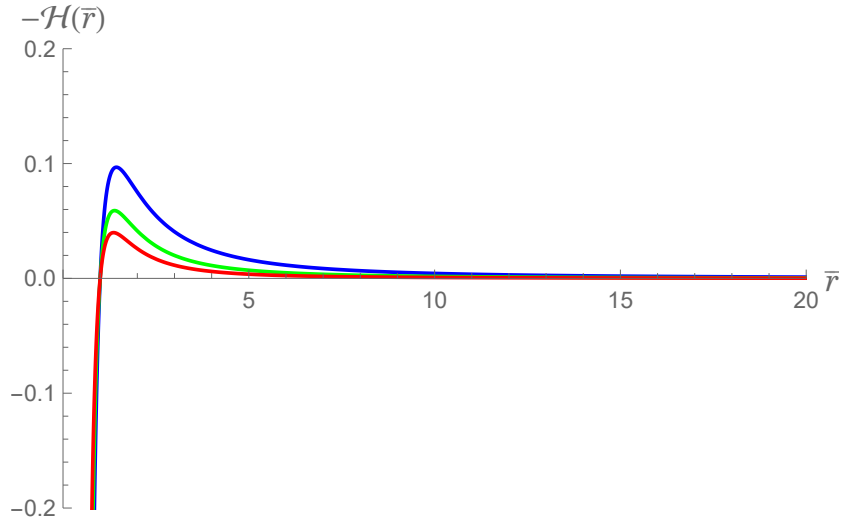


Figure 15: $-\mathcal{H}(\bar{r})$ for various charged Schwarzschild-Bach black holes using the parameters (45): blue ($q = 0$, $b = 0.3633018769168$), green ($q = 1$, $b = 1.02395913547716$), and red ($q = 2$, $b = 1.8348341584421$). This functions as an effective potential for null geodesics around the black hole.

See Figure 16, for the comparison of photon-sphere and black-hole-shadow radii, \bar{r}_{ps} and \bar{r}_{sh} , for various charged Schwarzschild and Schwarzschild-Bach black holes. Note that for highly charged Schwarzschild-Bach black holes, $\bar{r}_{\text{sh}} < \bar{r}_{\text{ps}}$. This is due to the negative lensing of light caused by negative mass of these black holes (see also Figure 19).

Finally, let us discuss the angular radius χ_{O} of the black-hole shadow (see Figure 17 and review [27]). Following [28], the angular radius of the black-hole shadow for a static observer at $\bar{r} = \bar{r}_{\text{O}}$ in

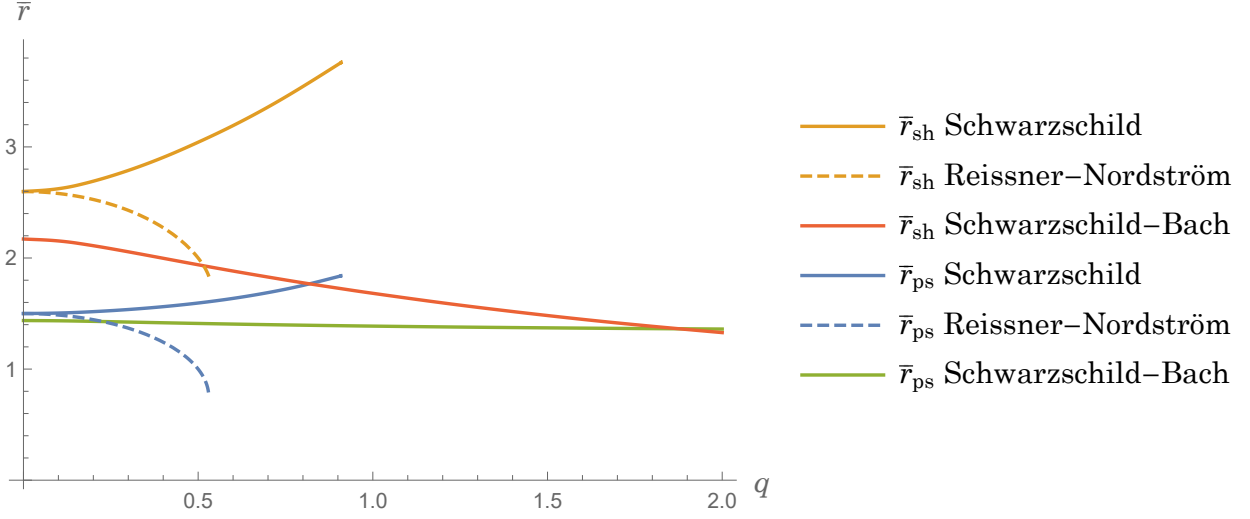


Figure 16: Radii \bar{r} of photon spheres and black hole shadows as functions of charge q and using the parameters (45). The photon spheres of charged Schwarzschild and Schwarzschild-Bach black holes correspond to the solid blue and green lines respectively; similarly, the solid yellow and red lines correspond to the respective shadows. The dashed lines correspond to the Reissner-Nordström black hole in contrast to the charged Schwarzschild solutions of quadratic gravity.

the static exterior region reads

$$\cot \chi_O = \sqrt{\frac{g_{\bar{r}\bar{r}}}{g_{\phi\phi}}} \frac{d\bar{r}}{d\phi}|_{\bar{r}=\bar{r}_O} = \frac{1}{\bar{r}\sqrt{f}} \frac{d\bar{r}}{d\phi}|_{\bar{r}=\bar{r}_O}, \quad \frac{d\bar{r}}{d\phi} = \pm \bar{r} \sqrt{f} \sqrt{\frac{\bar{r}^2 h(\bar{r}_{ps})}{\bar{r}_{ps}^2 h(\bar{r})} - 1}. \quad (52)$$

Thus

$$\sin^2 \chi_O = \frac{1}{1 + \cot^2 \chi_O} = \frac{\bar{r}_{ps}^2 h(\bar{r}_O)}{\bar{r}_O^2 h(\bar{r}_{ps})}, \quad (53)$$

which after using (13), simplifies to (see [17])⁷

$$\sin^2 \chi_O = \frac{\mathcal{H}(r_O)}{\mathcal{H}(r_{ps})}. \quad (54)$$

See Figures 18 and 19 for numerically integrated null geodesics for black holes in quadratic gravity with positive and negative mass, respectively.

Finally, let us show the dependence of the photon-sphere radius and black-hole shadow radius on asymptotic mass for uncharged (Figures 20 and 21) and charged (Figures 22 and 23) Schwarzschild and Schwarzschild-Bach black holes.

6 Extremal case $[0, 2]$

Finally, let us briefly comment on the case $[0, 2]$ describing geometry in the vicinity of the horizon of an extremal black hole.

⁷Note that in the limit $\bar{r}_O \rightarrow \infty$ (then $\sin^2 \chi_O \approx \frac{\bar{r}_{sh}^2}{\bar{r}_O^2}$) using the gauge such that $h(\bar{r}_O) = \bar{r}_O^2 \mathcal{H}(r_O) \rightarrow 1$, (54) leads to (51).

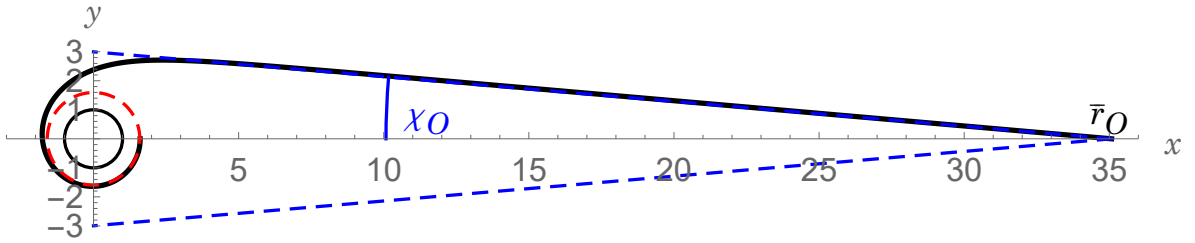


Figure 17: A critical null geodesic entering the photon sphere of a charged Schwarzschild black hole with the following parameters: $a_0 = 1$, $q = 0.5$, $b = -0.269102353931868$. The black circle and dashed, red circle indicate the event horizon and photon sphere respectively. An observer situated at \bar{r}_O will measure χ_O as the angular size of the black hole.

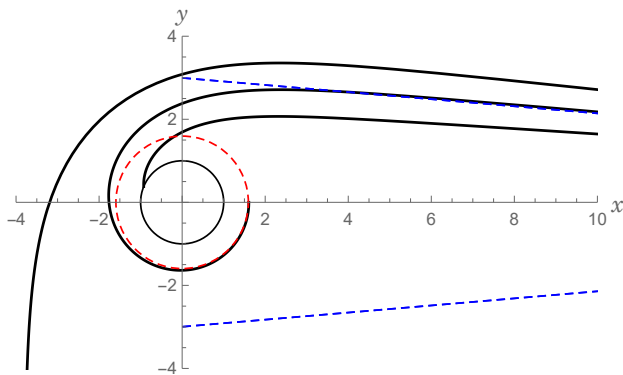


Figure 18: Null geodesics in the vicinity of a charged Schwarzschild black hole with the following parameters: $a_0 = 1$, $q = 0.5$, $b = -0.269102353931868$. Each passes through a distant point ($\bar{r} \approx 35$) where the fine-tuning of b is sufficient to maintain asymptotic-flatness. From this point, the projection of the angular shadow is indicated by the dashed, blue lines. The black circle and dashed, red circle indicate the event horizon and photon sphere, respectively.

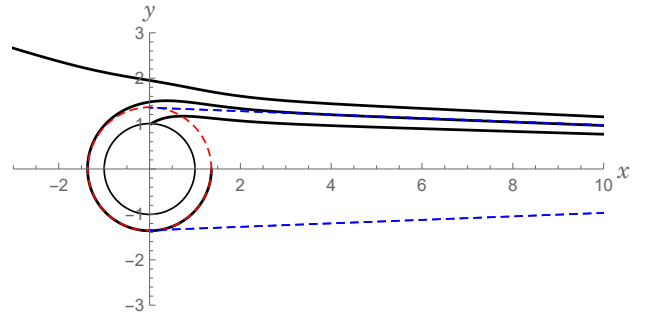


Figure 19: Null geodesics in the vicinity of a charged Schwarzschild-Bach black hole with the following parameters: $a_0 = 1$, $q = 2$, $b = 1.8348341584421$. Each passes through a distant point ($\bar{r} \approx 35$) where the fine-tuning of b is sufficient to maintain asymptotic flatness. From this point, the projection of the angular shadow is indicated by the dashed, blue lines. The black circle and dashed, red circle indicate the event horizon and photon sphere, respectively. It should be noted that the negative lensing of light not captured by the black hole is due to the negative mass of the highly charged Schwarzschild-Bach black hole.

Eq. (33) for $l = 0$ gives

$$c_0 = -1. \quad (55)$$

Then eq. (32) for $l = 0$ implies

$$a_0^2 = \frac{\kappa'}{2} q^2. \quad (56)$$

Thus this case can occur only for $q \neq 0$. This is in agreement with the results of [8, 16] in vacuum, where the [0,2] case is not allowed.

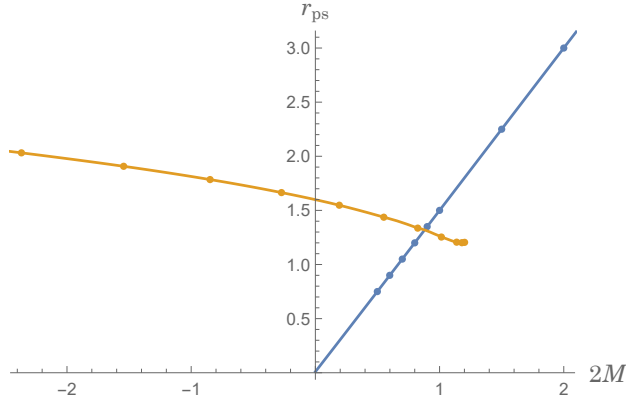


Figure 20: Radii of photon spheres for Schwarzschild (blue) and uncharged Schwarzschild-Bach (yellow) black holes as functions of asymptotic mass.

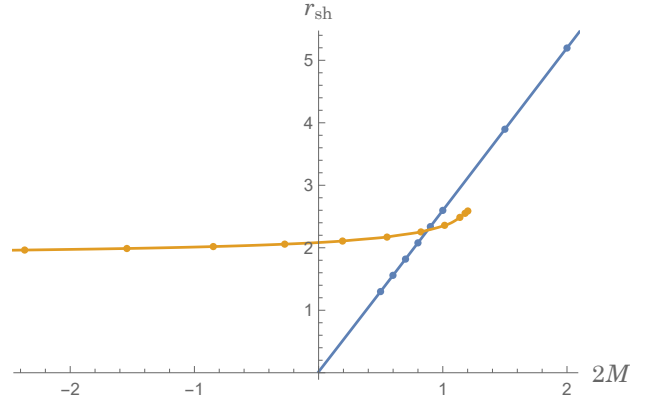


Figure 21: Radii of black hole shadows for Schwarzschild (blue) and uncharged Schwarzschild-Bach (yellow) black holes as functions of asymptotic mass.

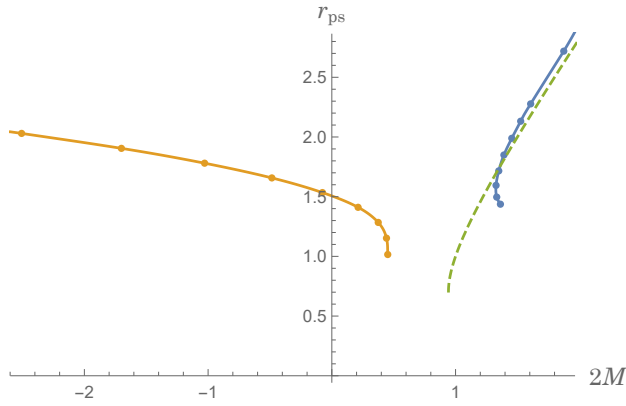


Figure 22: Radii of photon spheres for charged Schwarzschild (blue) and Schwarzschild-Bach (yellow) black holes with charge $q = 0.5$ as functions of asymptotic mass. The radii of Reissner-Nordström black hole photon spheres are indicated by the dashed green line.

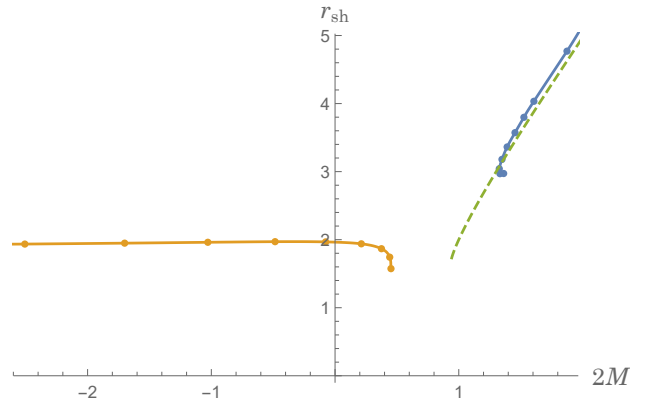


Figure 23: Radii of black hole shadows for charged Schwarzschild (blue) and Schwarzschild-Bach (yellow) black holes with charge $q = 0.5$ as functions of asymptotic mass. The radii of Reissner-Nordström black hole shadows are indicated by the dashed green line.

Eq. (32) for $l = 1$ implies

$$a_1 = \frac{a_0 c_1}{2}, \quad (57)$$

where c_1 is an integration constant. Therefore, $[0,2]$ is characterized by just 2 constants: a Bach parameter $b_2 \equiv c_1$ and charge q .

Then combining (31) and (32), for $l \geq 2$, we arrive at the recurrent relations

$$c_l = -6 \frac{(l+1)\mathcal{Y}_l + a_0(l-1)\mathcal{X}_l}{(l-1)(l+2)(l+1)[a_0^2 - 2kl(l+1)]}, \quad (58)$$

$$a_l = -\frac{a_0\mathcal{Y}_l + 2kl(l-1)\mathcal{X}_l}{l(l-1)[a_0^2 - 2kl(l+1)]}, \quad (59)$$

where

$$\mathcal{X}_l = \sum_{i=1}^{l-1} c_i a_{l-i} \left[(l-i)(l+1) + \frac{1}{6}(i+2)(i+1) \right], \quad (60)$$

$$\mathcal{Y}_l = \sum_{i=1}^{l-1} a_i a_{l-i} (l-i)(l-1-3i). \quad (61)$$

Near the extremal horizon, the Bach and Weyl invariants (15), (16) take the form

$$B_{ab}B^{ab}|_{r=r_h} = 2 \left(\frac{6}{\kappa'(\kappa'q^2 - 24k)} \right)^2 \left(\frac{b_2\Delta}{q} \right)^4 + \mathcal{O}(\Delta^5), \quad (62)$$

$$C_{abcd}C^{abcd}|_{r=r_h} = \frac{48b_2^2}{\kappa'^2q^4} \Delta^2 + \mathcal{O}(\Delta^3), \quad (63)$$

$$(64)$$

where $\Delta = r - r_h$ with r_h being the extremal horizon. Thus, similarly as for the Reissner-Nordström metric and in contrast with the [0,1] case, both the Bach and Weyl invariants vanish on the horizon.

We were not able to fine-tune the [0, 2] case to obtain an asymptotically flat solution. This might be related to the fact that the [0, 2] solution has less free parameters than the [0, 1] black holes.

6.1 Special cases with $c_1 = 0$

Note that the recurrent expressions (58)–(61) do not include special cases for which, in addition to (55), $c_1 = 0$ and $a_0^2 = \frac{\kappa'}{2}q^2 = 2kl(l+1)$ with $c_p = 0$, $p = 1, \dots, l-1$, and the only non-vanishing coefficients are $c_l \neq 0$ ($l \geq 2$), c_{lm} , and a_{lm} , $m = 1, 2, \dots$. The coefficients c_{lm} and a_{lm} are proportional to $(c_l)^m$.

In contrast with the generic [0, 2] solution, near the horizon, the Bach and Weyl invariants (15), (16) go to zero as

$$B_{ab}B^{ab}|_{r=r_h} \propto \frac{c_l^2}{a_0^8} \Delta^{2l}, \quad (65)$$

$$C_{abcd}C^{abcd}|_{r=r_h} \propto \frac{c_l^2}{a_0^4} \Delta^{2l}. \quad (66)$$

In physical coordinates, the power-series expansions of metric functions $f(\bar{r})$ and $h(\bar{r})$ (13) include fractional powers of $\bar{\Delta} = \bar{r} - a_0$ since $\bar{r} = \Omega = a_0 + a_l\Delta^l + \dots$ (12) and therefore $\Delta \propto \left(\frac{\bar{\Delta}}{a_l} \right)^{1/l}$.

Acknowledgements

We thank Marcello Ortaggio for helpful comments. This work has been supported by the Institute of Mathematics, Czech Academy of Sciences (RVO 67985840).

A Bach parameters required for asymptotic flatness

q	a_0	b (un)charged Schwarzschild	b (un)charged Schwarzschild-Bach
0	0.62	0	-0.589993571
0	0.65	0	-0.532684823
0	0.7	0	-0.42996068
0	0.8	0	-0.19860582
0	0.9	0	0.0660741
0	1	0	0.3633018769168
0	1.1	0	0.69267676
0	1.2	0	1.0539754
0	1.3	0	1.4470654
0	1.4	0	1.8718642
0	1.5	0	2.3283181
0.05	1	-0.00462	0.36791
0.1	1	-0.017831007	0.381097084
0.15	1	-0.03810	0.40132
0.2	1	-0.063682753	0.426841089
0.3	1	-0.1252725399	0.488250191
0.4	1	-0.19498743703	0.557709781
0.5	0.7		0.243104319
0.5	0.8	-0.5171222483	0.320022494
0.5	0.9	-0.3780781576	0.444080714
0.5	1	-0.269102353931868	0.6314924332806
0.5	1.1	-0.1939706824	0.885277714
0.5	1.2	-0.1447671171	1.19712757
0.5	1.3	-0.1121881706	1.5575176
0.5	1.4	-0.0898183758	1.95990043
0.5	1.5	-0.0738318916	2.40036761
0.5	1.8	-0.04584801196	
0.6	1	-0.345793969	0.7077718847
0.7	1	-0.4241119294	0.7855943886
0.8	1	-0.503525436775	0.86442570416
0.85	1	-0.54353900000085	
0.9	1	-0.583718480513498	0.94394733295808
0.91	1	-0.59177226034189	
1	1		1.02395913547716
1.2	1		1.18496948744475
1.4	1		1.34682262993053
1.6	1		1.5091937242
1.8	1		1.6719006501
2	1		1.8348341584421

Table 2: Fine-tuned Bach parameters b resulting in asymptotic flatness for a range of charged and uncharged Schwarzschild and Schwarzschild-Bach solutions. These values reflect the extent of fine-tuning carried out in this study and each value can undergo further tuning to achieve flatness at greater distances.

References

- [1] K. S. Stelle. Renormalization of higher-derivative quantum gravity. *Phys. Rev. D*, 16:953–969, 1977.
- [2] K. S. Stelle. Classical gravity with higher derivatives. *Gen. Rel. Grav.*, 9:353–371, 1978.
- [3] H. A. Buchdahl. On Eddington’s higher order equations of the gravitational field. *Proc. Edinburgh Math. Soc.*, 8:89–94, 1948.
- [4] H. A. Buchdahl. A special class of solutions of the equations of the gravitational field arising from certain gauge-invariant action principles. *Proc. Natl. Acad. Sci. U.S.A.*, 34:66–68, 1948.
- [5] H. Lü, A. Perkins, C. N. Pope, and K. S. Stelle. Black holes in higher derivative gravity. *Phys. Rev. Lett.*, 114:171601, 2015.
- [6] H. Lü, A. Perkins, C. N. Pope, and K. S. Stelle. Spherically symmetric solutions in higher derivative gravity. *Phys. Rev. D*, 92:124019, 2015.
- [7] H. Lü, A. Perkins, C. N. Pope, and K. S. Stelle. Lichnerowicz modes and black hole families in Ricci quadratic gravity. *Phys. Rev. D*, 96:046006, 2017.
- [8] J. Podolský, R. Švarc, V. Pravda, and A. Pravdová. Explicit black hole solutions in higher-derivative gravity. *Phys. Rev. D*, 98:021502, 2018.
- [9] R. Švarc, J. Podolský, V. Pravda, and A. Pravdová. Exact black holes in quadratic gravity with any cosmological constant. *Phys. Rev. Lett.*, 121:231104, 2018.
- [10] V. Pravda, A. Pravdová, J. Podolský, and R. Švarc. Black holes and other spherical solutions in quadratic gravity with a cosmological constant. *Phys. Rev. D*, 103:064049, 2021.
- [11] H. Lü, Y. Pang, C. N. Pope, and J. F. Vázquez-Poritz. AdS and Lifshitz black holes in conformal and Einstein-Weyl gravities. *Phys. Rev. D*, 86:044011, 2012.
- [12] A. Pravdová, V. Pravda, and M. Ortaggio. Topological black holes in higher derivative gravity. *Eur. Phys. J. C*, 83:180, 2023.
- [13] A. Held and J. Zhang. Instability of spherically symmetric black holes in quadratic gravity. *Phys. Rev. D*, 107(6):064060, 2023.
- [14] K. Lin, A. B. Pavan, G. Flores-Hidalgo, and E. Abdalla. New Electrically Charged Black Hole in Higher Derivative Gravity. *Braz. J. Phys.*, 47(4):419–425, 2017.

- [15] C. Wu, D. C. Zou, and M. Zhang. Charged black holes in the Einstein-Maxwell-Weyl gravity. *Nucl. Phys. B*, 952:114942, 2020.
- [16] J. Podolský, R. Švarc, V. Pravda, and A Pravdová. Black holes and other exact spherical solutions in quadratic gravity. *Phys. Rev. D*, 101:024027, 2020.
- [17] M. Ortaggio. A new look at AdS black holes with conformal scalar hair. 3 2024.
- [18] H. A. Buchdahl. On a set of conform-invariant equations of the gravitational field. *Proc. Edinburgh Math. Soc.*, 10:16–20, 1953.
- [19] W. Nelson. Static solutions for fourth order gravity. *Phys. Rev. D*, 82:104026, 2010.
- [20] V. Pravda, A. Pravdová, J. Podolský, and R. Švarc. Exact solutions to quadratic gravity. *Phys. Rev. D*, 95:084025, 2017.
- [21] B. Carter. Black hole equilibrium states. In C. De Witt and B. S. De Witt, editors, *Black holes*, pages 57–214. Gordon and Breach, New York, 1973.
- [22] T. Ortín. *Gravity and strings*. Cambridge University Press, Cambridge, second edition, 2015.
- [23] R. M. Wald. *General Relativity*. The University of Chicago Press, Chicago, 1984.
- [24] Z.-Y. Fan and H. Lü. Thermodynamical first laws of black holes in quadratically-extended gravities. *Phys. Rev. D*, 91:064009, 2015.
- [25] C.-M. Claudel, K. S. Virbhadra, and G. F. R. Ellis. The geometry of photon surfaces. *J. Math. Phys.*, 42:818–838, 2001.
- [26] H. Lu and Hong-Da Lyu. Schwarzschild black holes have the largest size. *Phys. Rev. D*, 101(4):044059, 2020.
- [27] V. Perlick and O. Y. Tsupko. Calculating black hole shadows: Review of analytical studies. *Phys. Rept.*, 947:1–39, 2022.
- [28] V. Perlick, O. Y. Tsupko, and G. S. Bisnovatyi-Kogan. Influence of a plasma on the shadow of a spherically symmetric black hole. *Phys. Rev. D*, 92(10):104031, 2015.